Electrochimica Acta 326 (2019) 134967

Contents lists available at ScienceDirect

Electrochimica Acta

journal homepage: www.elsevier.com/locate/electacta

Metal-free rGO/GO hybrid microelectrode array for sensitive and in-situ hydrogen peroxide sensing

Jing Zhang [a], Ming Zhao [b], Jun Yang [b], Gang Wu [a], Huaping Wu [c], Cen Chen [d], Aiping Liu [b, e, f, *]

[a] Department of Cardiovascular Medicine, Fourth Affiliated Hospital of Xinjiang Medical University, Urumqi, 830000, China
[b] Center for Optoelectronics Materials and Devices, Key Laboratory of Optical Field Manipulation of Zhejiang Province, Zhejiang Sci-Tech University, Hangzhou, 310018, PR China
[c] Key Laboratory of E&M (Zhejiang University of Technology), Ministry of Education & Zhejiang Province, Hangzhou, 310014, PR China
[d] College of Life Sciences, Zhejiang Sci-Tech University, Hangzhou, 310018, PR China
[e] State Key Laboratory for Strength and Vibration of Mechanical Structures, School of Aerospace Engineering, Xi'an Jiaotong University, Xi'an, 710049, PR China
[f] State Key Laboratory of Digital Manufacturing Equipment and Technology, Huazhong University of Science and Technology, Wuhan, 430074, PR China

ARTICLE INFO

Article history:
Received 18 August 2019
Received in revised form
26 September 2019
Accepted 27 September 2019
Available online 27 September 2019

Keywords:
Microelectrode array
Biosensor
Graphene derivative
H_2O_2 detection
Electrochemical catalysis

ABSTRACT

Microelectrode array (MEA) has recently attracted significant research interest in biomedical applications due to its high sensitivity, mass production and fast response. However, the previous MEA with precious metal-based nanomaterials for electro-catalysis may induce toxicity to cells. In this work, we present a metal-free graphene/graphene oxide (rGO/GO) hybrid MEA for precise and in-situ H_2O_2 secretion detection. The configuration and size of rGO/GO hybrid MEA can be well designed and controlled by combining the convenient lithography and electrochemistry method, where the GO region with abundant oxygen functionalized groups has good biocompatibility, so as to play as the adhesion and growth agent of pheochromocytoma cells (PC12 cells). Whereas, the rGO region with higher electro-catalytic activity can favor high sensitive in-situ H_2O_2 secretion detection that is released from the stimulated PC 12 cells at GO region, but with the cell filopodia extended to the rGO region. Besides, the rGO/GO hybrid MEA presented herein is compatible with the micro-fabrication technique and can be integrated into the lab-on-chip devices, which may shed useful insights for the design and fabrication of high performance biosensors.

1. Introduction

Detection of cell secretions, that can characterize cell activity and viability, is one of the most important methods for disease diagnose and precaution [1–3]. Among them, hydrogen peroxide (H_2O_2), as the most stable and general reactive oxygen species (ROS) generated by intracellular signaling molecules, such as hydroxyl radical (•OH), alkylperoxyl radical (ROO•), superoxide radical anion (O^{2-}), nitric oxide (NO), and peroxynitrite ($ONOO^-$), is being proved to play as a vital role in physiological signaling pathways through regulating DNA damage, cell apoptosis, protein synthesis, etc [4,5]. Meanwhile, emerging evidences further indicate that H_2O_2 is related to several kinds of physiological disorder, such as Parkinson's disease, atherosclerosis, Alzheimer's disease and cancer [6,7]. Therefore, the convenient and precise detection of H_2O_2 in viable cells is necessary not only for exploring its roles in cellular physiology, but also providing reliable diagnostic indicators for pathological analysis. In the past decades, electrochemical biosensors have been widely used for H_2O_2 detection [8]. Particularly, nanomaterials-based electrochemical biosensors, such as nanomaterials of noble metals like Pt, Au, Ag, metal sulfides like MoS_2, CuS, and metal oxides like Fe_2O_3, CuO, MnO_2 as alternative electrochemical catalysts, have been developed to construct non-enzymatic biosensors due to their rapid response, low cost, easy fabrication and high precision [9–13]. However, recent works have observed the toxicity and bioaccumulation of nanoparticles due to the releasing of metal ions or endocytosis of nanoparticles, which may significantly influence the cell proliferation, apoptosis, ROS

* Corresponding author. College of Life Sciences, Zhejiang Sci-Tech University, Hangzhou, 310018, PR China.
E-mail address: liuaiping1979@gmail.com (A. Liu).

https://doi.org/10.1016/j.electacta.2019.134967
0013-4686/

generation, etc [14]. Thus, one challenge of the nanomaterials-based electrochemical biosensors is to develop metal-free and biocompatible nanomaterials for cell culture and cell secretions detection.

Microelectrode array (MEA) has attracted significant research interest as electrochemical biosensors because of its high sensitivity, enhanced mass transfer, and large current response benefited from the device miniaturization [15]. Meanwhile, graphene or graphene oxide (GO), two-dimensional (2D) carbon material with heteroatoms, such as O, N, S, P, and trace metal impurities, has been extensively studied as alternative catalysts compared to noble metal catalysts due to its high chemical activity, long-term stability and low cost [16–19]. Reduced graphene oxide (rGO) prepared by Hummers' method with less oxygen functionalized groups and higher electric conductivity exhibits excellent electro-catalytic activity since the introduction of trace manganese and oxidation debris (OD) at the edges and basal plane of graphene sheet during oxidation and reduction processes [20,21]. However, previous works indicated graphene had some cytotoxicity to mammalian through characterizing the cell morphology, viability, and mortality under the environments with graphene. But, other works also showed GO containing abundant oxygen-containing groups, exhibits better biocompatibility than rGO because the sheet size, oxygen content, surface charge, and sharp edge of graphene and relative derivative have a strong impact on their biological/toxicological responses to mammalian cells [22,23]. Thus, exploring the biocompatibility, catalytic activity and electrochemical sensing ability of GO and rGO, and combining the advantages of GO and rGO, may provide new opportunities for constructing high-performance electrochemical biosensors.

In this work, we proposed the rGO/GO hybrid microelectrode array (rGO/GO hybrid MEA), which was not only a good incubator for pheochromocytoma cells (PC12) growth, but also a high-precision detector for in-situ detection of the cell secretion of H_2O_2. As illustrated in Scheme 1, the rGO/GO hybrid MEA was first fabricated on indium tin oxide (ITO) coated glass by combining the convenient lithography and electrochemistry method. The size, shape and pattern of GO/rGO hybrid MEA (rGO was surrounded by GO), and spacing between adjacent rGO electrodes were all programmable and well controlled without multi-mask design, which provided high freedom for cell culture and cell secretion detection. Most importantly and interestingly, when PC12 cells were seeded on rGO/GO hybrid MEA, the cells preferred to migrate and grow on GO surfaces with cell filopodia extended to rGO, which demonstrated the good biocompatibility of GO and provided rapid diffusion pathway of H_2O_2 (released from the stimulated PC12 cells at GO region) to rGO for further electrochemical detection.

2. Experimental section

2.1. Reagents and apparatus

Graphite powder, $KMnO_4$, H_2SO_4, H_3PO_4, HCl, ethanol, $NaH_2PO_4 \cdot 2H_2O$, $Na_2HPO_4 \cdot 7H_2O$, $K_4Fe(CN)_6$, $K_3Fe(CN)_6$, KCl and H_2O_2 (30 wt%) were purchased from Aladin Ltd. (Shanghai, China). ITO-coated glass slides with resistance of 8 Ω/square were supplied by Sigma. All of the other chemicals were of at least analytical grade and used without further purification. Aqueous solutions were prepared with deionized water. 0.2 M phosphate buffer solution (PBS, pH7.4) was prepared by mixing 19 mL NaH_2PO_4 solution (0.2 M) and 81 mL Na_2HPO_4 solution (0.2 M), and used as the supporting electrolyte in the electrochemical reduction of GO. 0.01 M PBS (pH7.4) was also prepared with the similar method and used as the supporting electrolyte for the detection of H_2O_2 secretion.

The morphology characterizations of rGO/GO hybrid MEA were carried out by VK-X100 laser microscope with a 680 nm wavelength laser light (Keyence Inc., Korea) and BX51 Optical Microscope (OLYMPUS, Japan). X-ray photoelectron spectroscopy (XPS) measurements were performed by the ESCALab220i-XL electron spectrometer from VG Scientific. Attenuated total reflection Fourier transform infrared spectroscopy (ATR-FTIR) was collected with the Thermo Scientific Nicolet 5700 spectrometer. Raman mapping was obtained on a Raman Microscope (Thermo DXR, USA) with a 632 nm wavelength laser light. The conductivity of GO and rGO was measured by using the four-point-probe technology via a Keithley 2400 Current/Voltage Source Meter with probe station. The contact angle measurement was carried out by the FTA1000 instrument (First Ten Angstroms, Portsmouth, VA). Electrochemical experiments were performed with the CHI 660D Electrochemical Workstation (Chenhua, China) at room temperature in a conventional three-electrode cell, equipped with an Ag/AgCl as reference electrode, a platinum wire as counter electrode, and the rGO/GO hybrid MEA attached on the ITO coated glass (6 mm × 9 mm) as working electrode.

2.2. Preparation of GO

GO was prepared from graphite powder by the modified Hummers' method [24]. Typically, a mixture of the concentrated H_2SO_4/H_3PO_4 solution (36 mL of H_2SO_4 and 4 mL of H_3PO_4) was slowly added to the mixture of graphite (0.3 g) and $KMnO_4$ (1.8 g). Then, the mixture was heated to 50 °C for further reaction of 12 h under continuous stirring. Next, 4 mL ice water with 30% H_2O_2 (0.5 mL) was carefully poured to the mixture and the suspension was further centrifuged twice (3000 rpm for 10 min). After that, the

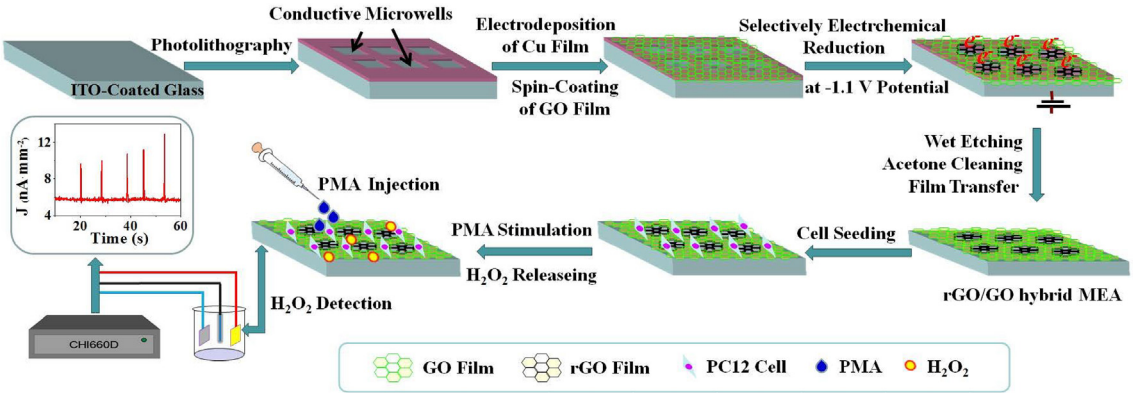

Scheme 1. Schematic illustration of the fabrication of rGO/GO hybrid MEA and in-situ H_2O_2 secretion detection.

remaining solid material was sequentially washed by deionized water, HCl and ethanol, respectively. Finally, GO powder was obtained by high-speed centrifugation and was washed with deionized water to neutral. Besides, further exfoliation was carried out by bath ultrasonication for 2 h to get the GO dispersion solution (3 mg/mL).

2.3. Fabrication of rGO/GO hybrid MEA

The fabrication of rGO/GO hybrid MEA was similar to our previous work [25], but some modifications were made. Briefly, in the lithography process, the photoresist was spin-coated on the ITO-coated glass surface at 8000 rpm for 7s to form a uniform photoresist layer with thicknesses of 600 nm. After ultraviolet exposure via the mask with patterns, some conductive microwells were obtained. Then, the GO aqueous solution (3 mg/mL) was spin-coated on the patterned substrate with electrodeposited copper film to form a uniform and continuous GO layer with thicknesses of 25 nm. Different rGO microarrays were obtained by electrochemically and selectively reducing the GO layer through the contacted copper microwells with different sizes, shapes and spacing for controllable time (Scheme 1). After wet etching in $FeCl_3$ solution and washing in acetone, the resulted film with rGO/GO hybrid MEA could be transferred to the desired substrates. Besides, the GO MEA as a controlled system was also prepared by spin-coating GO film on the ITO-coated glass surface, followed by lithography process via the mask with same patterns.

2.4. Cell culture

The PC12 cells were obtained from Chinese Academy of Shanghai Cell Bank. PC12 cells with density of 3×10^3/mL estimated by cell counter were seeded on the rGO/GO hybrid MEA, and further incubated in DMEM medium with 10% fetal bovine serum (FBS, Sigma, USA), 100 U/mL penicillin (Sigma, USA), and 100 mg/mL streptomycin (Sigma, USA) at a humid environment of 37 °C and 5% CO_2 for 24 h.

2.5. Evaluation of PC12 cell viability

In order to evaluate the PC12 cell viability, a common double staining method was used for the visualization of PC12 cell nuclei and F-actin filaments. First, PC12 cells were seeded on rGO/GO hybrid MEA, cultivated for 24 h, fixed with 3.7% paraformaldehyde in PBS, and permeabilized with 0.1% Triton X-100. Then, PC12 cells were further incubated for 30 min with 100 nM Acti-stain 555 fluorescent phalloidin (Cytoskeleton, USA) for the visualization of cytoplasmic F-actin in red color, and they were also stained with 5 μg/mL 40-6-diamidino-20-phenylindole (DAPI, Cytoskeleton, USA) for the visualization of cell nuclei in blue color. Finally, the cell nuclei and F-actin filaments were characterized by using the Fluorescence Microscope (OLYMPUS, Japan). Acti-stain 555 fluorescent phalloidin was excited at 550 nm and measured at 565–610 nm. DAPI fluorescence was excited at 405 nm and measured at 420 nm–480 nm.

2.6. Detection of H_2O_2 secretion

After 24 h incubation, the rGO/GO hybrid MEA with PC12 cells incubated on it was used for electrochemical measure in a three-electrode system in physiological 0.01 M PBS at the potential of 0.6 V, where the rGO/GO hybrid MEA was treated as the working electrode, as illustrated in Scheme 1. After obtaining the steady signal output as background current, 10 μL Phorbol 12-myristate 13-acetate (PMA, Sigma, USA) with concentration of 100 ng/mL was injected onto the rGO/GO hybrid MEA to stimulate H_2O_2 releasing of PC12 cells. Then, the released H_2O_2 was simultaneously monitored by rGO electrode. Besides, the signal output of rGO/GO hybrid MEA without PC12 cells under PMA stimulation was also tracked for reference.

3. Results and discussion

3.1. Characterization of rGO/GO hybrid MEA

The rGO/GO hybrid MEAs with different shapes, sizes and distribution of rGO patterns (such as the circular, equilateral triangular, square, hexagonal, crossing-linked and interdigitated ones) are well programmable and controlled by pre-designed masks, as shown in Fig. 1. We find that for 7 s reduction of GO, the shape and size of rGO pattern can exactly duplicate the mask ones [25]. Here, the rGO region exhibits darker color than that of GO due to the

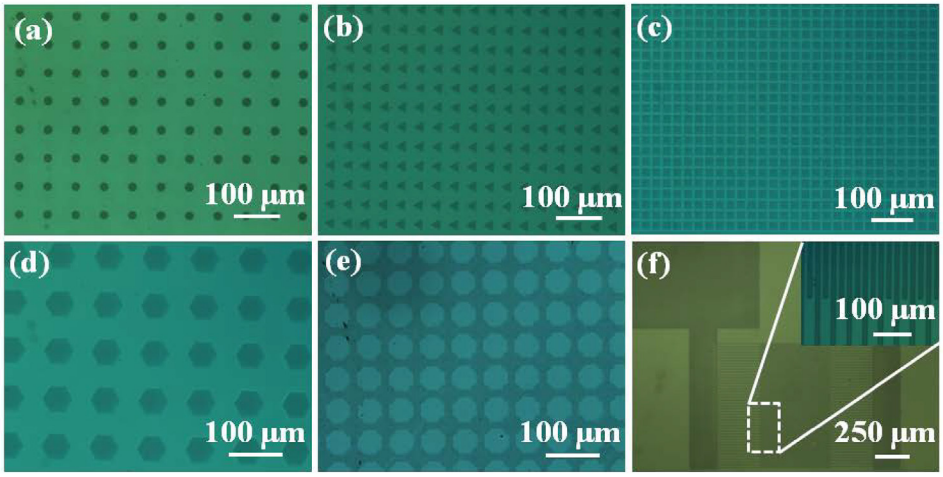

Fig. 1. Optical images of rGO/GO hybrid MEAs with GO reduction time of 7 s. (a) The circular rGO electrode array with diameter 20 μm and spacing 60 μm. (b) The equilateral triangular rGO electrode array with size 25 μm and spacing 25 μm. (c) The square rGO electrode array with size 20 μm × 20 μm and spacing 10 μm. (d) The hexagonal rGO electrode array with size 45 μm and spacing 45 μm. (e) The crossing-linked rGO electrode array with the junction diameter 30 μm and length of the connection cable 20 μm. (f) The interdigitated rGO electrode array with pitch width 25 μm and spacing 10 μm. The upper inset is the magnification of the dashed region in (f).

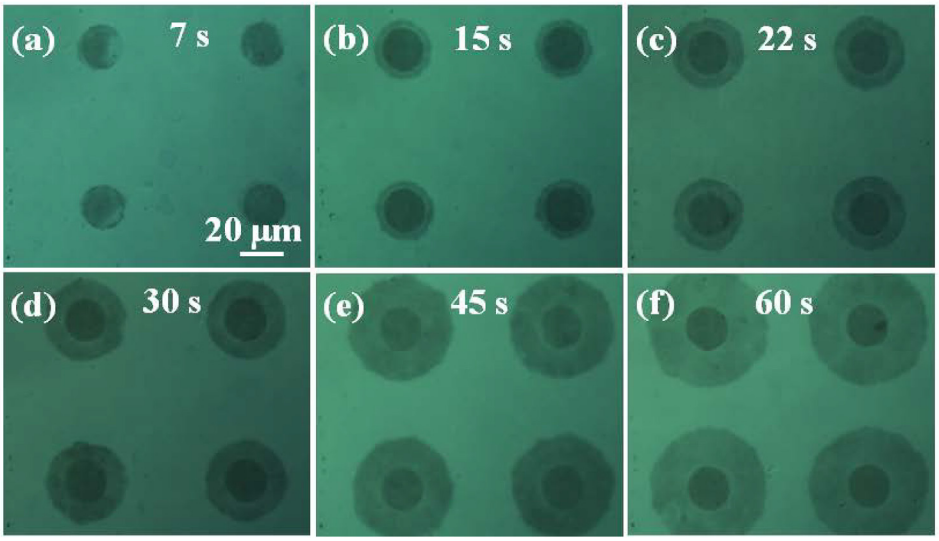

Fig. 2. (a–f) Optical images of circular rGO/GO hybrid MEAs with different reduction time from 7 s to 60 s. Here, the diameter of copper electrode is 20 μm and the 7 s reduction time can give the same size of rGO pattern.

deoxygenization after electrochemistry reduction [26].

Furthermore, the reduction time of GO will affect the size and distribution of rGO patterns. As shown in Fig. 2, with the increasing of reduction time from 7 s to 60 s, the dark region for the circular rGO electrode is gradually extended outward along the radial direction of the lithographic pattern, which means the size and distribution of rGO/GO hybrid MEA can be conveniently adjusted by only changing the reduction time of GO. Besides, the color of the later expanded rGO region is lighter than that of the initially contacted with the copper electrode region due to the smaller reduction degree [25]. This construction characteristic is also confirmed by XPS, FTIR and Raman measurements. From the XPS analysis of the rGO and GO region in rGO/GO hybrid MEA (Fig. 3a), we can see that the dominant peak near 287.4 eV in C1s spectrum of GO corresponds to the oxygen functionalized groups such as epoxy, hydroxyl, carbonyl or carboxyl [27], which would provide GO with good hydrophility and biocompatibility. However, this peak intensity is obviously weakened after 7s reduction with a drastic increase in the peak near 285.1 eV, which indicates the partially returning to the aromatic carbon structure after electrochemical reduction [27]. Further increasing of the reduction time results in slight change of the ratio of two peak intensities ($I_{287.4}/I_{285.1}$). The intensity of O 1s spectra also shows a similar trend (Fig. 3b). The FTIR data in Fig. 3c demonstrate that the oxygen functionalized groups in GO, such as the C═O bond at 1731 cm^{-1} and C–OH bond at 1224 cm^{-1}, disappear in rGO after only 7 s electrochemical reduction of GO. The intensity ratio of D band at 1345 cm^{-1} to G band at 1594 cm^{-1} (I_D/I_G) in the Raman spectra gradually increases from 0.97 for GO to 1.68 for 60s-reduced rGO due to the removing of oxygen functional groups and recovering of graphitic carbon

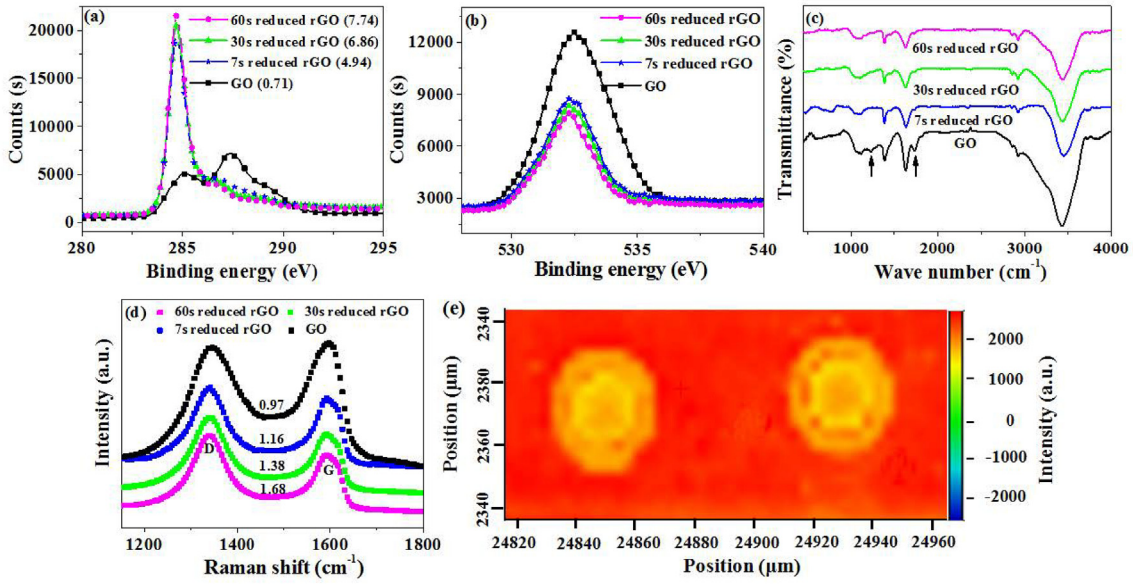

Fig. 3. (a) C1s, (b) O 1s, (c) FTIR and (d) Raman spectra of GO and rGO with different reduction time. The intensity ratio of the two peaks at 287.4 eV and 285.1 eV in the C1s spectrum ($I_{287.4}/I_{285.1}$) increases from 0.71 for GO to 7.74 for 60s-reduced rGO. The intensity ratio of D band at 1345 cm^{-1} to G band at 1594 cm^{-1} (I_D/I_G) in the Raman spectra increases from 0.97 for GO to 1.68 for 60s-reduced rGO. (e) Raman mapping of the D band for the rGO/GO hybrid MEA in Fig. 2(d).

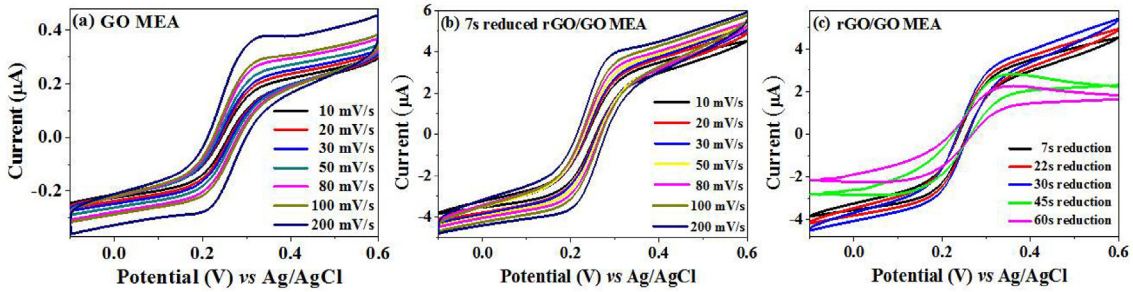

Fig. 4. Cyclic voltammograms of (a) GO MEA, (b) 7s-reduced rGO/GO hybrid MEA and (c) rGO/GO hybrid MEAs with different reduction time in 0.1 M KCl solution with 2 mM $Fe(CN)_6^{3-/4-}$. The scan rate changes from 10 mV/s to 200 mV/s in (a) and (b). The rGO/GO hybrid MEA used in (b) and (c) is shown in Fig. 2. The scan rate in (c) is 10 mV/s.

rings (Fig. 3d) [25]. Besides, the Raman mapping of D band of rGO/GO hybrid MEA (reduction time 30 s, Fig. 2d) presents clear interface between the GO and rGO regions (Fig. 3e), demonstrating the precisely controlled electrochemical reduction of GO, so as to the rGO pattern in the rGO/GO hybrid MEA. The intensity of D band of rGO in the original copper electrode region is slightly different from that of the later expanded region due to the different reduction degree. The four-point-probe electric conductivity measurement of the rGO on quartz substrates also shows an obvious effect of electrochemical reduction time. The rGO conductivity demonstrates an increase of at least three orders of magnitude from the GO film with an electrical conductivity of 4.4×10^{-3} Sm^{-1} to about 20–60 Sm^{-1} after electrochemical reduction for 7–60 s due to the removing of oxygenated groups [25]. The easy and controllable adjusting of electrical conductivity of rGO microarrays by changing GO reduction time provides the rGO/GO hybrid MEA potential applications for electrochemical sensor.

3.2. Electrochemical properties of the rGO/GO hybrid MEA

We further investigated the electrochemical property of rGO/GO hybrid MEA by using $Fe(CN)_6^{3-/4-}$ redox couple as the probe. Fig. 4a

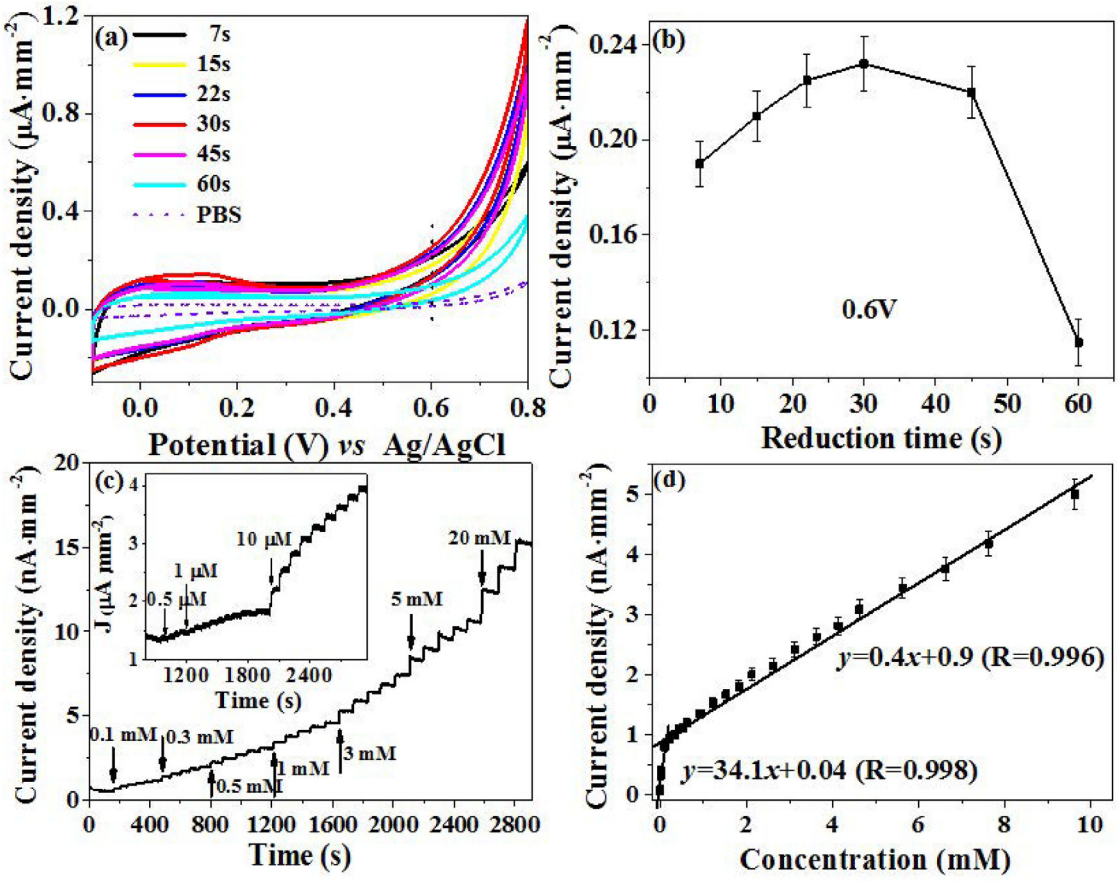

Fig. 5. (a) CVs of the rGO/GO hybrid MEAs with different reduction time in 0.01 M phosphate buffer (pH 7.4) and 20 mM H_2O_2. The scan rate is 50 mV/s. (b) Current density of the rGO/GO hybrid MEAs at 0.6 V. The error bars represent the standard deviation of six measurements by using six samples. (c) The current density output for 30s-reduced rGO/GO hybrid MEA at 0.01 PBS (pH 7.4) with sequentially adding different concentrations of H_2O_2 (the constant potential of 0.6 V is applied). (d) The relation between the current density of H_2O_2 oxidation and H_2O_2 concentration. The error bars represent the standard deviation of six measurements by using six samples.

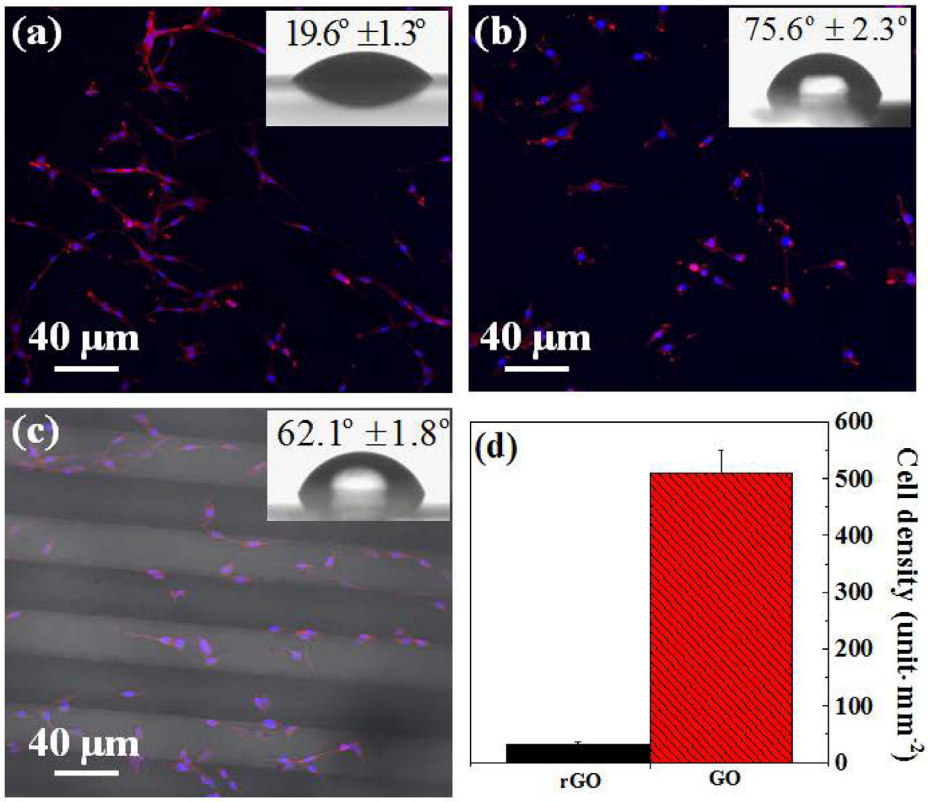

Fig. 6. PC12 cell adhesion and proliferation on (a) GO film, (b) 30s reduced rGO film, and (c) 30s-reduced rGO/GO hybrid MEA with rGO strip width 30 μm and spacing 30 μm after cell culture for 24 h. The PC12 cells were stained with Acti-stain 555 phalloidin (red color) and DAPI (blue color) to show the distribution of F-actin (cell skeletons) and cell nucleus. The insets in (a)–(c) are the contact angles of water on the surface of these samples. (d) The PC12 cell density on GO and rGO regions for the 30s-reduced rGO/GO hybrid MEA. Error bars represent standard deviations for six samples. (For interpretation of the references to color in this figure legend, the reader is referred to the Web version of this article.)

illustrates the cyclic voltammograms (CVs) of the GO MEA under different scan rates from 10 mV/s to 200 mV/s, indicating a radial diffusion regime at lower scan rates and a mixed regime at higher scan rates [28,29]. By contrast, the CV curves of the 7s-reduced rGO/GO hybrid MEA under different scan rates exhibit typical sigmoidal curves with current approximately 15 times larger than that of GO MEA (Fig. 4b), due to the partial recovery of π conjugation in rGO to increase its in-plane electron transfer kinetics [30,31]. The steady-state current is well kept for the rGO/GO hybrid electrode until the potential scan rate up to 200 mV/s, demonstrating a typical behavior of MEA. Furthermore, the MEA-like behavior for the rGO/GO hybrid electrode is still remained as the increasing of reduction time of GO. But, for the reduction time larger than 45 s, an obvious decreasing of the current signal is observed due to the overlapping of the diffusion zone of adjacent microelectrodes similar to that of macro electrode, as shown in Fig. 4c.

In order to evaluate the electro-catalytic activity of rGO/GO hybrid MEA for H_2O_2 oxidation, the CV tests were carried out in a three-electrode system including 20 mM H_2O_2 and 0.01 M PBS (pH = 7.4). Note that there is almost no current response in the electrolyte solution (0.01 M PBS, pH = 7.4) without H_2O_2 molecules (Fig. 5a). While, when the H_2O_2 molecules are added in the PBS, an obvious increase of current density is observed due to H_2O_2 oxidation, indicating the electro-catalytic activity of the rGO/GO hybrid MEAs. Here, the area of the hybrid electrodes with different reduction time is calculated according to the rGO parts through the optical images of the rGO/GO hybrid MEAs in Fig. 2. As the electro-catalysis of H_2O_2 oxidation mostly occurs for the voltage larger than 0.4 V, and the oxygen generation becomes dominating over the voltage of 0.7 V, we compare the current density of H_2O_2 oxidation for the rGO/GO hybrid MEAs with different reduction time at the point of 0.6 V. It can be seen that the maximum current density is obtained for 30s-reduced rGO/GO hybrid MEA (Fig. 5b). This phenomenon demonstrates that the careful design of rGO/GO hybrid MEAs with appropriate structure defect, oxygen functionalized groups, distribution, pattern, and electrical conductivity can optimize their electro-catalytic activity for H_2O_2 oxidation [32]. Therefore, the 30s-reduced rGO/GO hybrid MEA is used in the following study. The chronoamperometric curve was measured at the potential of 0.6 V to calibrate the measuring range and sensitivity of the rGO/GO hybrid MEA for H_2O_2 detection. When different amount of H_2O_2 was discontinuously injected onto the hybrid MEA, the stepwise increasing of the current density is observed for H_2O_2 concentration from 0.5 μM to 20 mM (Fig. 5c), which suggests the metal-free rGO/GO hybrid MEA could detect H_2O_2 in a wide range from micromolar to tens of millimolar. The relation between the current density and H_2O_2 concentration is shown in Fig. 5d, which demonstrates a wide linear range over H_2O_2 concentration. The sensitivity of this sensor for H_2O_2 detection is 34.1 $nAmm^{-2}mM^{-1}$ in the concentration ranging from 1.0 μM to 1.0 mM ($R = 0.998$) and 0.4 $nAmm^{-2}mM^{-1}$ in the concentration ranging from 1.0 mM to 9.6 mM ($R = 0.996$). The higher sensitivity at lower H_2O_2 concentration may be caused by the higher diffusivity and catalytic activity of H_2O_2 at lower concentration due to the limited diffusion channel and catalytic site of the rGO/GO hybrid MEA. The detection limit of H_2O_2 for the rGO/GO hybrid MEA is estimated to be 0.18 μM by assuming the ratio of signal-to-noise (S/N = 3). Thus, the metal-free rGO/GO hybrid MEA exhibits comparable performance to that of

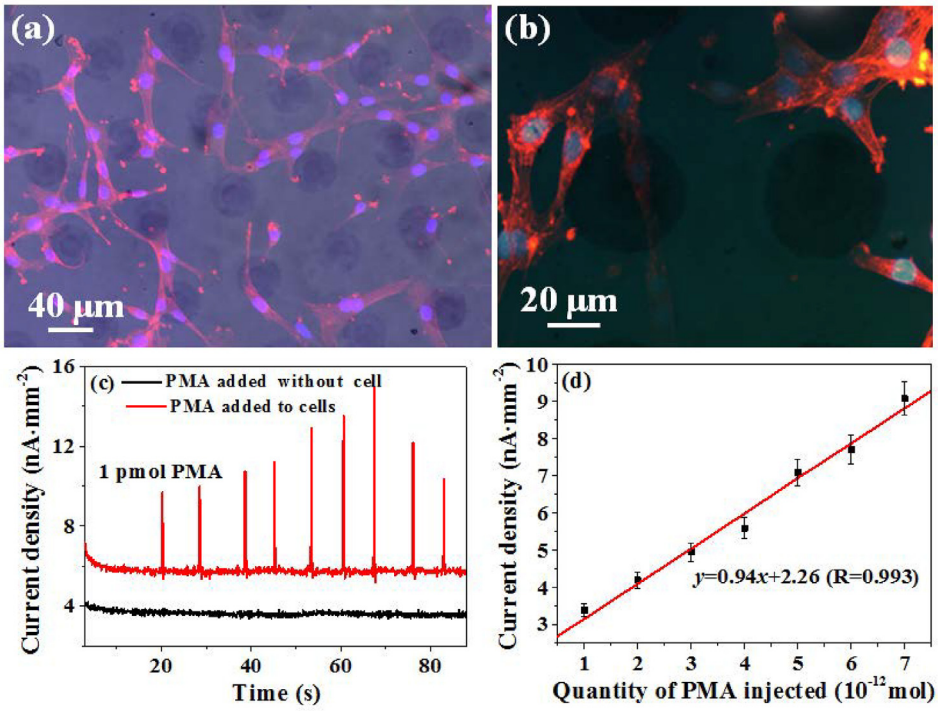

Fig. 7. (a) PC12 cells adhesion on 30s-reduced rGO/GO hybrid MEA (Fig. 2d) after cell culture for 24 h. (b) Local magnification of the PC12 cells adhered on 30s-reduced rGO/GO hybrid MEA. The PC12 cells were stained with Acti-stain 555 phalloidin (red color) and DAPI (blue color) to show the distribution of F-actin (cell skeletons) and cell nucleus. (c) In-situ H_2O_2 secretion detection on 30s-reduced rGO/GO hybrid MEA under PMA stimulus (100 nM) in 0.01 M PBS (pH7.4) at the applied potential of 0.6V. (d) The relation of the oxidation current density to the quantity of injected PMA. The error bars represent the standard deviation for six measurements by using six samples. (For interpretation of the references to color in this figure legend, the reader is referred to the Web version of this article.)

the H_2O_2 biosensors with nano-composites or precious metals reported before [33,34].

3.3. PC12 cell growth and H_2O_2 secretion detection

Graphene and its derivatives have attracted great research interest for their potential applications in biosensor and biomedical applications. However, the toxicity and biocompatibility is one of the most concerned issues for graphene related biomedical applications. Here, we first study the wettability of the rGO/GO hybrid MEA. The contact angle was measured by dropping a 10 μL deionized water on the sample surface and recording the image with a digital camera. As shown in the inset of Fig. 6a, the GO film is of good hydrophility with contact angle about 19.6° due to the abundant oxygen functionalize groups [35]. When GO film was electrochemically reduced for 30 s, the obtained rGO film shows a contact angle about 75.6° as the deoxygenization decreases the polarity (the inset in Fig. 6b). While for the 30s-reduced rGO/GO hybrid MEA (rGO strip with width 30 μm and spacing 30 μm), the contact angle is about 62.1° due to the synergic effect of GO and rGO parts (the inset in Fig. 6c). In general, the adhesion and proliferation of PC12 cells are significantly affected by surface wetting properties. Thus, PC12 cells are well spreading on GO surface with the filopodia unfolded and outspread after seeding for 24 h (Fig. 6a). While the PC12 cells on 30s-reduced rGO surface show shrunk configuration (Fig. 6b). The difference is attributed to the hydrophilic surface of GO with abundant oxygen functionalized groups, so that it is more biocompatible than that of rGO. For the 30s-reduced rGO/GO hybrid MEA with strip-like pattern (rGO strip of width 30 μm and spacing 30 μm), the PC12 proliferation demonstrates interesting phenomenon. When the cell nucleus was stained with DAPI (blue color) and F-actin was stained with Acti-stain 555 phalloidin (red color), we can clearly observe that most of the cell nucleus are distributed on the GO region, while the F-actin is uniformly stretched along the strip direction and located at the GO side (Fig. 6c). More interesting, most of the cell filopodia are extended to the interface of GO and rGO, which can be ascribed to the edge effect and rough interface between GO and rGO so as to provide numerous anchoring sites for PC12 cell filopodia spreading, as reported by Kim and Yang [36,37]. The histogram of cell density on GO and rGO parts for 30s-reduced rGO/GO hybrid MEA (Fig. 6d) further verified the preferred cell migration and proliferation on GO surface.

Because of the good biocompatibility and high sensitivity of the rGO/GO hybrid MEA, it can be used for in-situ H_2O_2 secretion detection of PC12 cells (seeding density of 50000 cells/cm^2). Fig. 7a and (b) depict the status of the PC12 cells grew on 30s-reduced rGO/GO hybrid MEA (Fig. 2d), which indicates that most of PC12 cells prefer to grow on the GO region with the filopodia extending to the interface of rGO and GO, i.e. PC 12 cell are closely surrounding the circular rGO electrode. Upon exposure to PMA, ROS are formed in PC12 cells, resulting in apoptosis [38]. Fig. 7c shows the current density output of the 30s-reduced rGO/GO hybrid MEA treated with 10 μL of 100 nM PMA for nine times. In comparison, there is only reference current output for the rGO/GO hybrid MEA without PC12 cells. In the case with the PC 12 cell culture, a sharp current impulse is immediately obtained for each PMA stimulation addition and then the signal comes back to baseline within 2 s. This can be explained that when the PMA is added to the near-surface of rGO/GO hybrid MEA, the H_2O_2 is instantly released from the filopodia of the simulated cells and promptly oxidized on the rGO/GO hybrid MEA at the applied potential of 0.6V. Since the amount of released H_2O_2 is relative low, the cell filopodia extended to the interface of rGO and GO provides

fast diffusion channels for the H_2O_2 secretion to the conductive and electrochemical active rGO region for rapid and sensitive H_2O_2 detection in a very short time. About 3.9 nA mm^{-2} peak current density is recorded for the first PMA stimulus. As the further increasing of PMA stimulus, the peak current density increases until the 7th stimulus (Fig. 7d), corresponding to the increasing of H_2O_2 releasing due to the ROS generation under PMA stimulus [9]. However, further PMA stimulus (8th and 9th) may cause apoptosis or falling off of PC12 cells, resulting in the decreasing of current output (Fig. 7c). The relation of the current output to the amount of injected PMA is shown in Fig. 7d, and a linear relation is obtained.

4. Conclusion

In this work, we proposed the metal-free rGO/GO hybrid MEAs for sensitive and in-situ H_2O_2 secretion detection. By combining the convenient lithography and electrochemistry method, the size, shape and pattern of rGO/GO hybrid MEAs were all programmable and well controlled. Because of the good hydrophilicity of GO (partially due to the abundant oxygen functionalized groups) and high electro-catalytic activity of rGO, the rGO/GO hybrid MEA exhibited high sensitivity for H_2O_2 detection with H_2O_2 concentration ranging from 0.18 μM to 9.6 mM. On the other hand, the rGO/GO hybrid MEA also exhibited good biocompatibility for PC12 cells proliferation and growth with cell filopodia extending to the interface of GO and rGO, which provided rapid diffusion channel for H_2O_2 secretion oxidation. The rGO/GO hybrid MEA with comparable sensor performance to that of the nanocomposites or precious metals based biosensors, are compatible with the microfabrication technique and can be easily integrated to the lab-on-chip devices, which may shed useful insights for the design and fabrication of high-performance biosensors.

Acknowledgments

This work was supported by the National Natural Science Foundation of China (No. 51175472), the Zhejiang Outstanding Youth Fund (No. LR19E020004), the Opening Fund of State Key Laboratory for Strength and Vibration of Mechanical Structures (Xi'an Jiaotong University) (No. SV2018-KF-23) and the Opening Fund of State Key Laboratory of Digital Manufacturing Equipment and Technology (Huazhong University of Science and Technology) (No. DMETKF2018017).

References

[1] Y. Liu, Z. Matharu, A. Rahimian, A. Revzin, Detecting multiple cell-secreted cytokines from the same aptamer-functionalized electrode, Biosens. Bioelectron. 64 (2015) 43–50.
[2] M.P. Raphael, J.A. Christodoulides, J.B. Delehanty, J.P. Long, J.M. Byers, Quantitative imaging of protein secretions from single cells in real time, Biophys. J. 105 (2013) 602–608.
[3] S.M. Roper, M. Zemskova, B.A. Neely, A. Martin, P. Gao, E.E. Jones, A.S. Kraft, R.R. Drake, Targeted glycoprotein enrichment and identification in stromal cell secretomes using azido sugar metabolic labeling, Proteom. Clin. Appl. 7 (2013) 367–371.
[4] N.F. Cruz, K.K. Ball, G.A. Dienel, Astrocytic gap junctional communication is reduced in amyloid-beta-treated cultured astrocytes, but not in Alzheimer's disease transgenic mice, ASN Neuro 2 (2010), e00041.
[5] W.Z. Xu, Y. Xing, J. Liu, H.P. Wu, Y. Cui, D.W. Li, D.Y. Guo, C.Y. Li, A.P. Liu, H. Bai, Efficient water transport and solar steam generation via radially, hierarchically structured aerogels, ACS Nano 13 (2019) 7930–7938.
[6] F. Pagliari, C. Mandoli, G. Forte, E. Magnani, S. Pagliari, G. Nardone, S. Licoccia, M. Minieri, P. Di Nardo, E. Traversa, Cerium oxide nanoparticles protect cardiac progenitor cells from oxidative stress, ACS Nano 6 (2012) 3767–3775.
[7] P. Wu, Z. Cai, Y. Gao, H. Zhang, C. Cai, Enhancing the electrochemical reduction of hydrogen peroxide based on nitrogen-doped graphene for measurement of its releasing process from living cells, Chem. Commun. 47 (2011) 11327–11329.
[8] C. Zhu, G. Yang, H. Li, D. Du, Y. Lin, Electrochemical sensors and biosensors based on nanomaterials and nanostructures, Anal. Chem. 87 (2015) 230–249.
[9] F. Xiao, J.B. Song, H.C. Gao, X.L. Zan, R. Xu, H.W. Duan, Coating graphene paper with 2d-assembly of electrocatalytic nanoparticles: a modular approach toward high-performance flexible electrodes, ACS Nano 6 (2012) 100–110.
[10] Y. Zhang, X. Bai, X. Wang, K.K. Shiu, Y. Zhu, H. Jiang, Highly sensitive graphene-Pt nanocomposites amperometric biosensor and its application in living cell H2O2 detection, Anal. Chem. 86 (2014) 9459–9465.
[11] J. Bai, X. Jiang, A facile one-pot synthesis of copper sulfide-decorated reduced graphene oxide composites for enhanced detecting of H2O2 in biological environments, Anal. Chem. 85 (2013) 8095–8101.
[12] T. Wang, H. Zhu, J. Zhuo, Z. Zhu, P. Papakonstantinou, G. Lubarsky, J. Lin, M. Li, Biosensor based on ultrasmall MoS2 nanoparticles for electrochemical detection of H2O2 released by cells at the nanomolar level, Anal. Chem. 85 (2013) 10289–10295.
[13] L. Li, Z. Du, S. Liu, Q., Hao, Y. Wang, Q. Li, T. Wang, A novel nonenzymatic hydrogen peroxide sensor based on MnO2/graphene oxide nanocomposite, Talanta 82 (2010) 1637–1641.
[14] K.L. Aillon, Y. Xie, N. El-Gendy, C.J. Berkland, M.L. Forrest, Effects of nanomaterial physicochemical properties on in vivo toxicity, Adv. Drug Deliv. Rev. 61 (2009) 457–466.
[15] F. Li, M. Xue, X. Ma, M. Zhang, T. Cao, Facile patterning of reduced graphene oxide film into microelectrode array for highly sensitive sensing, Anal. Chem. 83 (2011) 6426–6430.
[16] Y. Song, K. Qu, C. Zhao, J. Ren, X. Qu, Graphene oxide: intrinsic peroxidase catalytic activity and its application to glucose detection, Adv. Mater. 22 (2010) 2206–2210.
[17] Y. Jiao, Y. Zheng, M. Jaroniec, S.Z. Qiao, Origin of the electrocatalytic oxygen reduction activity of graphene-based catalysts: a roadmap to achieve the best performance, J. Am. Chem. Soc. 136 (2014) 4394–4403.
[18] X.H. Wang, A.P. Liu, Y. Xing, H. W Duan, W.Z. Xu, Q. Zhou, H.P. Wu, C. Chen, B.Y. Chen, Three-dimensional graphene biointerface with extremely high sensitivity to single cancer cell monitoring, Biosens. Bioelectron. 105 (2018) 22–28.
[19] M. Yuan, A.P. Liu, M. Zhao, W.J. Dong, T.Y. Zhao, J.J. Wang, W.H. Tang, Bimetallic PdCu nanoparticle decorated three-dimensional graphene hydrogel for non-enzymatic amperometric glucose sensor, Sens. Actuators B 190 (2014) 707–714.
[20] A. Bonanni, A. Ambrosi, C.K. Chua, M. Pumera, Oxidation debris in graphene oxide is responsible for its inherent electroactivity, ACS Nano 8 (2014) 4197–4204.
[21] L. Wang, A. Ambrosi, M. Pumera, Metal-free" catalytic oxygen reduction reaction on heteroatom-doped graphene is caused by trace metal impurities, Angew. Chem., Int. Ed. Engl. 52 (2013) 13818–13821.
[22] Y. Chang, S.T. Yang, J.H. Liu, E. Dong, Y. Wang, A. Cao, Y. Liu, H. Wang, In vitro toxicity evaluation of graphene oxide on A549 cells, Toxicol. Lett. 200 (2011) 201–210.
[23] K.H. Liao, Y.S. Lin, C.W. Macosko, C.L. Haynes, Cytotoxicity of graphene oxide and graphene in human erythrocytes and skin fibroblasts, ACS Appl. Mater. Interfaces 3 (2011) 2607–2615.
[24] D.C. Marcano, D.V. Kosynkin, J.M. Berlin, A. Sinitskii, Z. Sun, A. Slesarev, L.B. Alemany, W. Lu, J.M. Tour, Improved synthesis of graphene oxide, ACS Nano 4 (2010) 4806–4814.
[25] M. Zhao, A. Liu, H. Wu, B. Wu, C. Li, W. Tang, Electrochemistry-assisted microstructuring of reduced graphene oxide-based microarrays with adjustable electrical behavior, Electrochem. Commun. 48 (2014) 86–90.
[26] H. Teoh, Y. Tao, E. Tok, G. Ho, C. Sow, Electrical current mediated interconversion between graphene oxide to reduced grapene oxide, Appl. Phys. Lett. 98 (2011) 173105.
[27] D.R. Dreyer, S. Park, C.W. Bielawski, R.S. Ruoff, The chemistry of graphene oxide, Chem. Soc. Rev. 39 (2010) 228–240.
[28] A.M. Ng, Y. Wang, W.C. Lee, C.T. Lim, K.P. Loh, H.Y. Low, Patterning of graphene with tunable size and shape for microelectrode array devices, Carbon 67 (2014) 390–397.
[29] M.C. Henstridge, R.G. Compton, Mass Transport to micro-and nanoelectrodes and their arrays: a review, Chem. Rec. 12 (2012) 63–71.
[30] Y. Matsumoto, M. Koinuma, S.Y. Kim, Y. Watanabe, T. Taniguchi, K. Hatakeyama, H. Tateishi, S. Ida, Simple photoreduction of graphene oxide nanosheet under mild conditions, ACS Appl. Mater. Interfaces 2 (2010) 3461–3466.
[31] M. Zhou, Y. Zhai, S. Dong, Electrochemical sensing and biosensing platform based on chemically reduced graphene oxide, Anal. Chem. 81 (2009) 5603–5613.
[32] A.M.H. Ng, Kenry, C. Teck Lim, H.Y. Low, K.P. Loh, Highly sensitive reduced graphene oxide microelectrode array sensor, Biosens. Bioelectron. 65 (2015) 265–273.
[33] M. Liu, R. Liu, W. Chen, Graphene wrapped Cu2O nanocubes: non-enzymatic electrochemical sensors for the detection of glucose and hydrogen peroxide with enhanced stability, Biosens. Bioelectron. 45 (2013) 206–212.
[34] Z. Wen, S. Ci, J. Li, Pt nanoparticles inserting in carbon nanotube arrays: nanocomposites for glucose biosensors, J. Phys. Chem. C 113 (2009) 13482–13487.
[35] J. Rafiee, M.A. Rafiee, Z.Z. Yu, N. Koratkar, Superhydrophobic to superhydrophilic wetting control in graphene films, Adv. Mater. 22 (2010) 2151–2154.
[36] M.T. Yang, J. Fu, Y.-K. Wang, R.A. Desai, C.S. Chen, Assaying stem cell

mechanobiology on microfabricated elastomeric substrates with geometrically modulated rigidity, Nat. Protoc. 6 (2011) 187–213.
[37] D.-H. Kim, K. Han, K. Gupta, K.W. Kwon, K.-Y. Suh, A. Levchenko, Mechanosensitivity of fibroblast cell shape and movement to anisotropic substratum topography gradients, Biomaterials 30 (2009) 5433–5444.
[38] H. Takei, A. Araki, H. Watanabe, A. Ichinose, F. Sendo, Rapid killing of human neutrophils by the potent activator phorbol 12-myristate 13-acetate (PMA) accompanied by changes different from typical apoptosis or necrosis, J. Leukoc. Biol. 59 (1996) 229–240.